患者が手の運動野に刺入された100極の刺入電極からのスパイク活動でディスプレイ画面上のカーソルを自在にコントロールできることを報告している[6]. Hochbergらは2012年には脳幹出血後遺症で四肢麻痺の患者がロボットアームをコントロールして，机の上のボトルをつかんで口元まで持って行き中に入っているジュースを飲むことに成功したと，報告している[7]. 2013年になってSchwartzらは四肢麻痺の患者が13週間のトレーニングの後，さらに巧緻なロボットアーム制御ができるようになったことを発表している[8].

しかし，刺入電極は脳実質に致して侵襲性があり，電極の刺入により惹起される炎症反応により数カ月単位で計測効率が低下する．信号が劣化しにくい電極の開発が進められているが，明確な解決策は見つかっていない状況である．

皮質脳波は脳表面に直接皿状電極をおいて計測される脳波であり，頭皮脳波に比較してノイズが少なく，高周波帯域まで計測できるという特徴がある．また脳実質への侵襲が比較的少なく，長期間にわたる信号安定性に優れている．

理研の藤井らはサルに硬膜下電極を約1年間にわたり埋込んで実験を行った結果，皮質脳波で上肢の運動の3次元位置を電極留置期間中ずっと正確に推定できること，また一旦コンピュータに運動パターンを学習させると，再学習なしに半年にわたって正確な3次元位置推定ができることを明らかにした[9]. これは皮質脳波の長期安定性を示しており，臨床応用する上では最も重要な要素でもある．

海外の報告では，1次元の位置推定が2004年に報告されて以降，皮質脳波の研究報告が増えている．その後2次元の位置推定が複数のグループから報告され[10,11]，これを用いてカーソル制御ができたとの報告がある[12]. 運動推定に関しては指のレベルでの判別が可能との報告がある[13]. また通常の臨床で用いられる硬膜下電極は電極間隔は約1cmであるが，精度向上のためにこれを数mm程度に高密度化したmicroECoG電極に関する報告もある[14-16]. 最近では脊髄損傷で四肢麻痺の患者でカーソルやロボットアームの3次元制御を達成したとの症例報告がなされている[17].

我々も皮質脳波を用いてBMIの研究に取り組んでおり，これまでに，中心溝内運動野の皮質脳波が運動内容推定に有用なことを明らかにし，γ帯域活動を用いたロボットハンドのリアルタイム制御に成功し，運動障害の程度が強くても運動イメージ時のγ帯域活動を用いると運動内容推定が可能であることを明らかにしてきた．以下に我々の研究成果を概説する．

A. Support vector machineを用いた運動内容推定

難治性疼痛に対する運動野電気刺激療法の最適刺激部位同定や，難治性てんかんのてんかん焦点源同定のために硬膜下電極を2週間程度留置する場合がある．また難治性疼痛に対する運動野電気刺激療法において，より効果的疼痛緩和を目的として中心溝内に電極を留置する場合がある[18]. 我々は施設内倫理委員会の承認を得て，これまでにこうした症例対象にして，留置した電極から上肢運動等の課題施行時の皮質脳波を計測し，BMIの研究を行ってきた．

運動企図や運動内容の推定を行うneural decoding（脳信号解読）はBMIの中心となる技術であり，種々の手法が報告されているが，私どもはsupport vector machine（SVM）という機械学習の手法を中心に用いている．

大脳における運動内容の最終出力部は一次運動野であるが，体性局在があり，ヒトでは一次運動野は中心前回から中心溝の前壁にかけて存在すると考えられている．そこでこれらの部位をカバーする電極を用いて上肢運動時の皮質脳波を計測

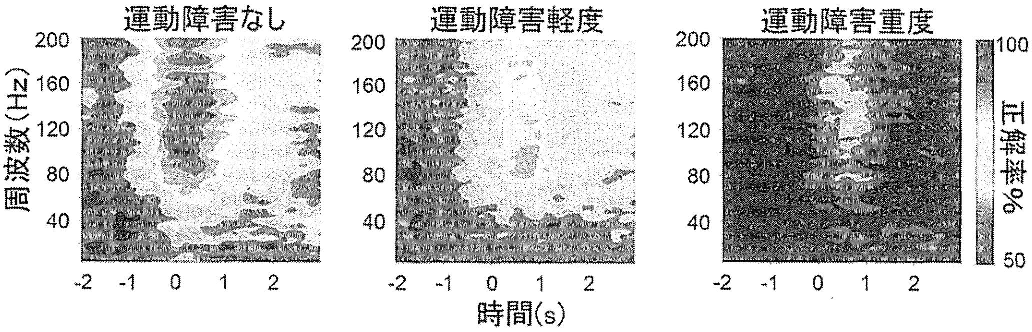

図1　運動障害の程度と運動内容推定正解率の関係

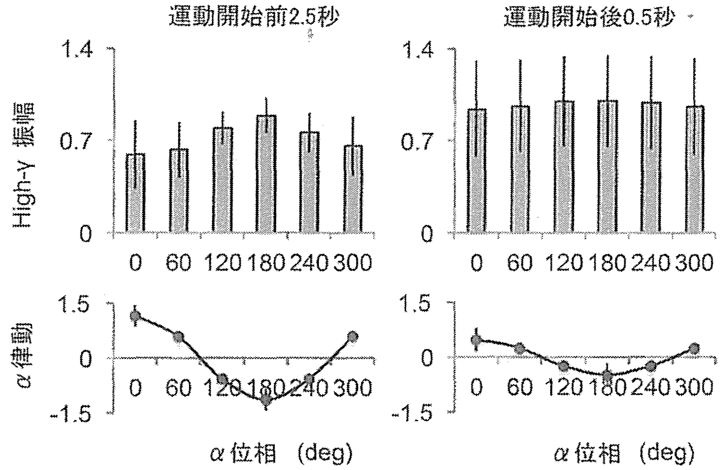

図2　運動野では運動前にγ帯域の振幅がα帯域の位相にカップリングする
α帯域の位相が180°の時に，γ帯域の振幅が大きくなっている．

し，SVMを用いて運動内容推定を行った．その結果，中心溝前壁から記録した皮質脳波を用いると，他の部位よりも有意に高い正解率で運動内容推定ができることが明らかになった[19]．

またどの周波数帯域が運動内容推定に有用であるかを調べた．その結果，γ帯域（80～150Hz）のパワーが運動内容推定に有用であることを明らかになった[20]．さらに被験者の運動障害の有無によらず，γ帯域のパワーを用いると高い運動内容推定の正解率が得られることが明らかになった（図1）[21]．運動障害の強い症例では，握る，肘を曲げるという運動のイメージが明確にできる被験者では握る，肘を曲げるという2つの運動で，γ波活動の脳内分布に明確な違いが認められたが，運動イメージがしにくいと自覚している被験者では，γ波活動の脳内分布に有意な差を認めなかった．これは，被験者がどれくらい違う運動イメージを自覚してできるかということと，脳内で実際どれくらい違った活動パターンになっているかということが，対応していることを示唆しており，脳機能の再構築に関する知見として興味深い．

さらに最近では，運動制御メカニズムに関する新しい知見を得ている．手の把握時に，運動野において運動開始前にγ帯域活動の振幅がα帯域活

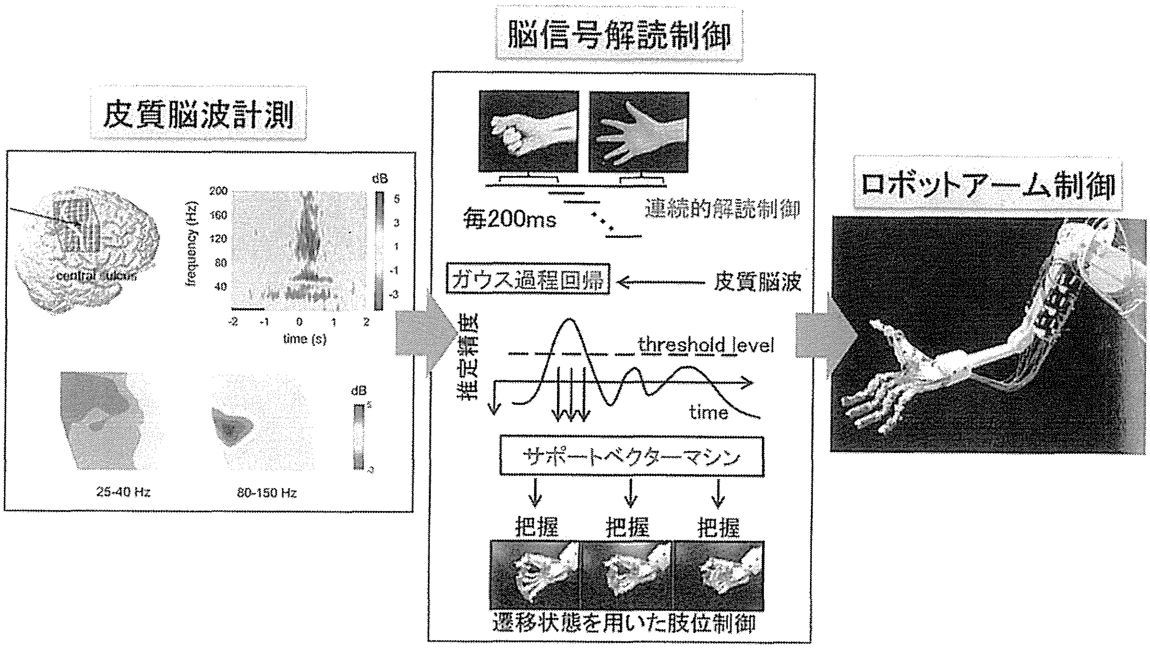

図3　リアルタイムロボットアーム制御

動の位相に同期し，運動開始直前に同期がはずれる現象（cross frequency coupling）を発見した(図2)[22]．手の把握において，このcross frequency couplingは運動開始や運動内容の制御に関わっていることを示唆する重要な知見といえる．

B. ロボットアームのリアルタイム制御

前項で述べた運動内容推定技術を応用して義手ロボットをリアルタイムに制御するシステムを開発した（図3)[21]．このシステムでは手の把握，つまむ，開くや肘の屈曲といった基本的な上肢の運動要素を各40回程度行い，これをSVMの学習データとしてパラメータ設定を行い，次にそのパラメータ設定を用いてリアルタイムに連続的なdecodingと制御を行う．Gaussian process regressionという手法を用いて計測した脳信号に対して運動推定がどの程度正確にできるかを随時評価し，運動推定が正確にできると評価された時に限り，SVMによるdecodingを行うことにより，外乱ノイズに強いdecodingができるようにしている．さらにロボットアームの制御に遷移状態の概念を導入して，初期肢位から目的肢位に徐々に状態遷移させることによりスムーズな動作にすることができた．これらの結果，運動1回毎の皮質脳波による運動の推定精度は60～80％でも，ロバストな運動推定・ロボット制御法を導入することにより，手から肘までの制御や，物の把握や把握解除など実用的な動作ができるようになった．また，硬膜下電極を用いた皮質脳波計測は長期間安定していることが動物実験で明らかになっている．我々の臨床例でも約2週間という短期間の電極留置のため長期の安定性は検証困難であるが，初回の実験から4日後でも初回の設定パラメータを利用して，リアルタイムロボットアーム制御により，物体の把握・把握解除ができることを示せた．

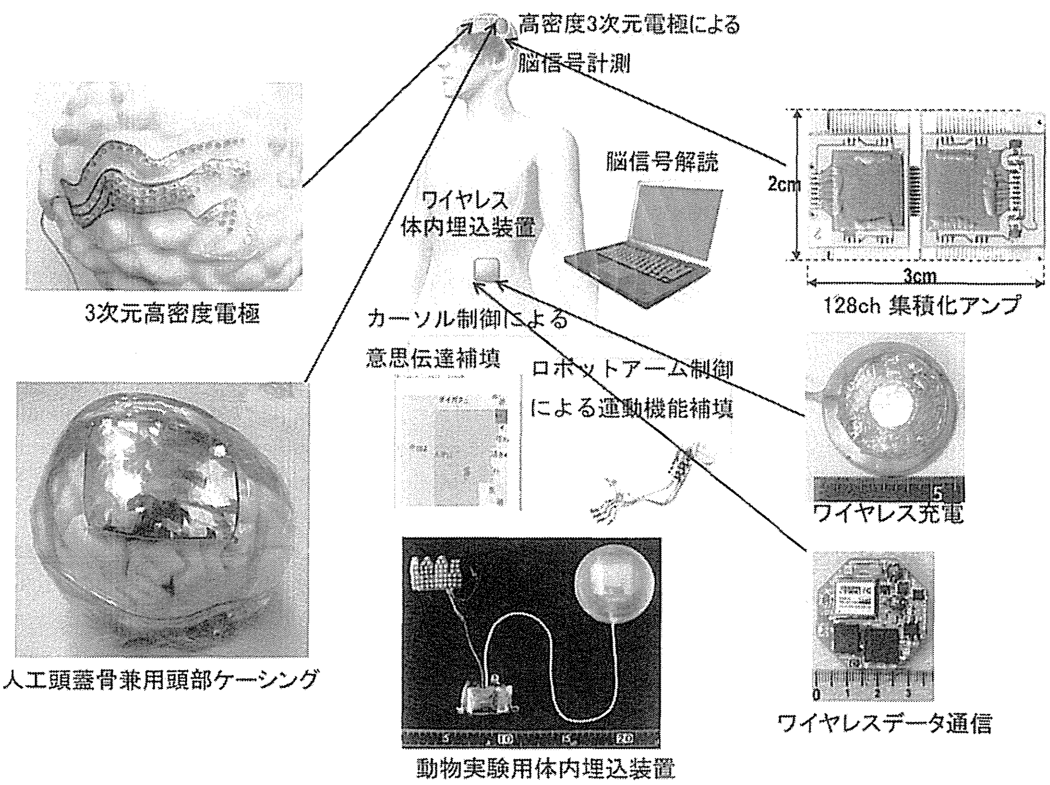

図4　ワイヤレス体内埋込装置

C．重症ALS患者を対象とした有線での BMI臨床研究

前述した成果にもとづいて，重症ALS患者を対象として，新たに開発した3次元高密度両面電極を3週間留置して，皮質脳波を用いた運動機能・意思伝達支援システムを評価する臨床研究を開始している．これは人工呼吸器管理下にある最重症のALS患者3名を対象としており，主評価項目を安全性，副次評価項目を上肢運動推定の正解率，ロボットアームの制御能，意思伝達能としている．現在1例目の評価が終了したところである．

D．ワイヤレス体内埋込装置の開発

侵襲型BMIでは臨床応用に際しては感染リスク低減のためにワイヤレス体内埋込化が必須であるが，一旦体内に埋め込むと装置の頻回の装脱着・調整の必要がなく利便性に優れる．BMIの臨床用ワイヤレス埋込装置はまだ報告が少なく，Kennedyらのグループが報告している埋込装置は電極数2チャンネルであり[23]，ブラウン大学のグループが開発中の装置も32チャンネルと，まだ測定チャンネル数も少ない[24]．動物実験やヒトでの有線でのロボットアーム制御では100チャンネルレベルのシステムを用いていることを考えると，これらの装置はスペック的に十分とは言いにくい面がある．そこで現在我々は電極数100チャンネル以上の臨床用ワイヤレス体内埋込BMI装置の実用化を目指して現在開発を行っており，プロトタイプを試作した（図4）[25]．本装置は頭部装置と腹部装置からなる．頭部装置は，

3次元高密度両面電極，128チャンネル集積化アンプとアンプを収納する人工頭蓋骨兼用頭部ケーシングからなる．腹部装置は，低電力消費型ワイヤレスLANデータ通信回路，非接触充電電源からなる．現在，その有用性や安全性を検証するために，動物実験を開始したところである．ごく最近になり，海外からも64チャンネルや100チャンネルの埋込装置が発表され始めており，今後の動向が注目される[26,27]．

実用化においては，埋込装置が開発されるとBMIとしての用途以外に，脳波計として用いて難治性てんかんの焦点源同定などへの応用も考えられる．

むすび

本稿では侵襲型BMIの動向について概説し，ついで我々が開発を進めている皮質脳波を用いた低侵襲BMIを紹介した．侵襲型BMIは体内埋込装置を用いた高性能の機能代替技術として，臨床応用が期待される．まずはALSなどの稀少疾患ではあるが最重症の身体障害への臨床応用を目指し，技術の進歩により性能が向上すれば，脊髄損傷，切断肢，脳卒中後遺症など障害の程度は低いが患者数が多い疾患にも適用が可能になると考えられ，医療機器としての潜在的市場規模は大きい．また埋込装置は，BMI用以外にも埋込脳波計として臨床応用が可能であり，より患者数の多い難治性てんかんを対象とすることにより，着実な臨床応用が可能となろう．

〈謝辞〉

本項で紹介した研究の一部は文部科学省の脳科学研究戦略推進プログラム「日本の特長を活かしたBMIの統合的研究開発」，厚生労働省の厚生労働科学研究費補助金医療技術実用化総合研究事業，文部科学省の橋渡し研究加速ネットワークプログラム，ならびに日本学術振興会の科学研究費補助金23390347により行われている．

文献

1) Wessberg J, Stambaugh CR, Kralik JD, et al. Real-time prediction of hand trajectory by ensembles of cortical neurons in primates. Nature. 2000; 408: 361-5.
2) Serruya MD, Hatsopoulos NG, Paninski L, et al. Instant neural control of a movement signal. Nature. 2002; 416: 141-2.
3) Taylor DM, Tillery SI, Schwartz AB. Direct cortical control of 3D neuroprosthetic devices. Science. 2002; 296: 1829-32.
4) Georgopoulos AP, Kalaska JF, Caminiti R, et al. On the relations between the direction of two-dimensional arm movements and cell discharge in primate motor cortex. J Neurosci. 1982; 2: 1527-37.
5) Velliste M, Perel S, Spalding MC, et al. Cortical control of a prosthetic arm for self-feeding. Nature. 2008; 453: 1098-101.
6) Hochberg LR, Serruya MD, Friehs GM, et al. Neuronal ensemble control of prosthetic devices by a human with tetraplegia. Nature. 2006; 442: 164-71.
7) Hochberg LR, Bacher D, Jarosiewicz B, et al. Reach and grasp by people with tetraplegia using a neurally controlled robotic arm. Nature. 2012; 485: 372-5.
8) Collinger JL, Wodlinger B, Downey JE, et al. High-performance neuroprosthetic control by an individual with tetraplegia. Lancet. 2013; 381: 557-64.
9) Chao ZC, Nagasaka Y, Fujii N. Long-term asynchronous decoding of arm motion using electrocorticographic signals in monkeys. Front Neuroengineering. 2010; 3: 3.
10) Schalk G, Kubanek J, Miller KJ, et al. Decoding two-dimensional movement trajectories using electrocorticographic signals in humans. J Neural Eng. 2007; 4: 264-75.
11) Pistohl T, Ball T, Schulze-Bonhage A, et al. Prediction of arm movement trajectories from ECoG-recordings in humans. J Neurosci Methods. 2008; 167: 105-14.
12) Schalk G, Miller KJ, Anderson NR, et al. Two-

dimensional movement control using electrocorticographic signals in humans. J Neural Eng. 2008; 5: 75-84.

13) Miller KJ, Zanos S, Fetz EE, et al. Decoupling the cortical power spectrum reveals real-time representation of individual finger movements in humans. J Neurosci. 2009; 29: 3132-7.

14) Wang W, Degenhart AD, Collinger JL, et al. Human motor cortical activity recorded with Micro-ECoG electrodes, during individual finger movements. Conf Proc IEEE Eng Med Biol Soc. 2009; 2009: 586-9.

15) Van Gompel JJ, Stead SM, Giannini C, et al. Phase I trial: safety and feasibility of intracranial electroencephalography using hybrid subdural electrodes containing macro- and microelectrode arrays. Neurosurg Focus. 2008; 25: E23.

16) Kellis SS, House PA, Thomson KE, et al. Human neocortical electrical activity recorded on nonpenetrating microwire arrays: applicability for neuroprostheses. Neurosurg Focus. 2009; 27: E9.

17) Wang W, Collinger JL, Degenhart AD, et al. An electrocorticographic brain interface in an individual with tetraplegia. PLoS One. 2013; 8: e55344.

18) Hosomi K, Saitoh Y, Kishima H, et al. Electrical stimulation of primary motor cortex within the central sulcus for intractable neuropathic pain. Clin Neurophysiol. 2008; 119: 993-1001.

19) Yanagisawa T, Hirata M, Saitoh Y, et al. Neural decoding using gyral and intrasulcal electrocorticograms. Neuroimage. 2009; 45: 1099-106.

20) Yanagisawa T, Hirata M, Saitoh Y, et al. Real-time control of a prosthetic hand using human electrocorticography signals. J Neurosurg. 2011; 114: 1715-22.

21) Yanagisawa T, Hirata M, Saitoh Y, et al. Electrocorticographic control of a prosthetic arm in paralyzed patients. Ann Neurol. 2012; 71: 353-61.

22) Yanagisawa T, Yamashita O, Hirata M, et al. Regulation of motor representation by phase-amplitude coupling in the sensorimotor cortex. J Neurosci. 2012; 32: 15467-75.

23) Guenther FH, Brumberg JS, Wright EJ, et al. A wireless brain-machine interface for real-time speech synthesis. PLoS One. 2009; 4: e8218.

24) Aceros J, Yin M, Borton DA, et al. A 32-channel fully implantable wireless neurosensor for simultaneous recording from two cortical regions. Conf Proc IEEE Eng Med Biol Soc. 2011; 2011: 2300-6.

25) Hirata M, Matsushita K, Suzuki T, et al. A fully-implantable wireless system for human brain-machine interfaces using brain surface electrodes: W-HERBS. IEICE Trans Commun. 2011; E94-B: 2448-53.

26) Borton DA, Yin M, Aceros J, et al. An implantable wireless neural interface for recording cortical circuit dynamics in moving primates. J Neural Eng. 2013; 10: 026010.

27) Charvet G, Foerster M, Chatalic G, et al. A wireless 64-channel ECoG recording electronic for implantable monitoring and BCI applications: WIMAGINE. Conf Proc IEEE Eng Med Biol Soc. 2012; 2012: 783-6.

Prediction of Three-Dimensional Arm Trajectories Based on ECoG Signals Recorded from Human Sensorimotor Cortex

Yasuhiko Nakanishi[1,9], Takufumi Yanagisawa[2,3,4,9], Duk Shin[1*], Ryohei Fukuma[3], Chao Chen[1], Hiroyuki Kambara[1], Natsue Yoshimura[1], Masayuki Hirata[2], Toshiki Yoshimine[2], Yasuharu Koike[1]

1 Precision and Intelligence Laboratory, Tokyo Institute of Technology, Yokohama, Japan, 2 Department of Neurosurgery, Osaka University Medical School, Osaka, Japan, 3 ATR Computational Neuroscience Laboratories, Kyoto, Japan, 4 Division of Functional Diagnostic Science, Osaka University Graduate School of Medicine, Osaka, Japan

Abstract

Brain-machine interface techniques have been applied in a number of studies to control neuromotor prostheses and for neurorehabilitation in the hopes of providing a means to restore lost motor function. Electrocorticography (ECoG) has seen recent use in this regard because it offers a higher spatiotemporal resolution than non-invasive EEG and is less invasive than intracortical microelectrodes. Although several studies have already succeeded in the inference of computer cursor trajectories and finger flexions using human ECoG signals, precise three-dimensional (3D) trajectory reconstruction for a human limb from ECoG has not yet been achieved. In this study, we predicted 3D arm trajectories in time series from ECoG signals in humans using a novel preprocessing method and a sparse linear regression. Average Pearson's correlation coefficients and normalized root-mean-square errors between predicted and actual trajectories were 0.44~0.73 and 0.18~0.42, respectively, confirming the feasibility of predicting 3D arm trajectories from ECoG. We foresee this method contributing to future advancements in neuroprosthesis and neurorehabilitation technology.

Citation: Nakanishi Y, Yanagisawa T, Shin D, Fukuma R, Chen C, et al. (2013) Prediction of Three-Dimensional Arm Trajectories Based on ECoG Signals Recorded from Human Sensorimotor Cortex. PLoS ONE 8(8): e72085. doi:10.1371/journal.pone.0072085

Editor: Maurice Ptito, University of Montreal, Canada

Received April 18, 2013; **Accepted** July 4, 2013; **Published** August 21, 2013

Funding: This work was supported in part by KAKENHI grants (22390275, 23390347, and 24700419) from the Japan Society for the Promotion of Science (JSPS). A part of this study was the result of "Brain Machine Interface Development" carried out under the Strategic Research Program for Brain Sciences by the Ministry of Education, Culture, Sports, Science and Technology of Japan. The funders had no role in study design, data collection and analysis, decision to publish, or preparation of the manuscript.

Competing Interests: The authors have declared that no competing interests exist.

* E-mail: shinduk@cns.pi.titech.ac.jp

9 These authors contributed equally to this work.

Introduction

A number of prominent brain-machine interface studies have arisen, in which electroencephalography (EEG), magnetoencephalography (MEG), electrocorticography (ECoG), and intracortical microelectrode have been applied to neuroprosthesis control, neurorehabilitation and novel communication tools for paralyzed or "locked-in" patients suffering from neuromuscular disorders. Since EEG and MEG are non-invasive and have high temporal resolution, they have been used in various paradigms, such as online control of a computer cursor [1–2], direction inference of hand movements [3–5], operation of a spelling device [6], and neurofeedback for rehabilitation [7–13]. Although a large proportion of these non-invasive methods succeeded in classification of movement direction or intention, prediction of time-varying trajectories is likely difficult due to insufficient spatial resolution and low signal-to-noise ratio in such methods.

Signal recording with intracortical microelectrodes is a powerful tool to realize precise trajectory prediction or accurate device control. Using motor cortical signals in animals, studies have shown successful prediction of hand trajectories [14–16] and grasp types and velocity [17], control of a computer cursor [18] or a robot arm [19–22], and controlled stimulation to a paralyzed arm [23]. These techniques have also been applied in humans to control a cursor [24] and a virtual keyboard and virtual hand [25]. However, though intracortical electrodes can provide rich information for BMI control, they face limitations such as signal degradation due to glial scarring [26]and potential displacement from the recording site [27].

Conversely, ECoG is less invasive than microelectrodes and can offer higher spatial resolutions than EEG and MEG. Researchers have been applying ECoG in humans for several years now and in numerous applications. The classification of hand movement directions or grasp types [28–33], one-, two-, or three-dimensional cursor control [27,34–40], and prediction of finger flexion [41] are just some examples of ECoG applications in human patients. Studies concerning the prediction of three-dimensional (3D) trajectory or muscle activities from primate ECoG have shown outstanding results [42–45]. Investigations on the prediction of 3D arm trajectory using ECoG in humans, however, are lacking, despite the potential to provide significant improvement in neuroprosthesis and neurorehabilitation technology. The inadequate quality of ECoG signals recorded from patients is one potential obstacle in predicting 3D trajectories. Specifically, (1) paralyzed or elderly patients may find it difficult to perform a long series of repeating trials and stably replicate the same motion for

Table 1. Clinical profiles in patients who participated in this study.

No.	Age	Sex	Diagnosis (Left/Right)	Duration of disease	Paresis (MMT)	Sensation
1	64 yr.	Male	Thalamic hemorrhage (R)	7 yr.	Spastic (4)	Hypoesthesia
2	65 yr.	Male	Ruptured spinal dural arteriovenous fistula	8 yr.	Spastic (4)	Hypoesthesia
3	14 yr.	Male	Intractable epilepsy (R)	7 yr.	None	Normal

doi:10.1371/journal.pone.0072085.t001

each trial, (2) ECoG signals in patients can include pathological activity, depending on the condition, and (3) the electrode sites on the cortex and the recording lengths can differ, depending on the treatment.

The aim of this study was to predict 3D arm trajectories from ECoG time series in human patients as a basis for a neuroprosthesis. Patients diagnosed with thalamic hemorrhage, ruptured spinal dural arteriovenous fistula (dAVF) and intractable epilepsy executed rotating tasks with three objects on a table. We simultaneously recorded arm trajectories and ECoG signals from 15~60 electrodes on the sensorimotor cortex. Using a novel method, we predicted four joint angles for the shoulder and elbow joints and six coordinates for the elbow and wrist joints in patients with different pathology.

Materials and Methods

Ethics Statement

The study was approved by the ethics committee of Osaka University Hospital (Approval No.08061) and conducted in accordance with the Declaration of Helsinki. ECoG electrodes were embedded not for our experiments but for patients' medical treatments. Written informed consent was obtained before initiating any research procedures. All patients or their guardians gave written informed consent for the use of their data in the academic study.

Participants

Three patients (males; 14–64 years) participated in our study (Table 1). Patients 1 and 2 had spastic paresis and weakness in the left arm due to stroke. Their sensorimotor cortices were undamaged, though moderate motor dysfunction was observed. The youngest participant, patient 3, was diagnosed with intractable epilepsy but did not show motor dysfunction. As part of their treatments, all participants were implanted with subdural electrode arrays (Unique Medical Co., Tokyo, Japan) covering the sensorimotor cortex, including the central sulcus. The arrays remained implanted in the intracranium for two weeks to determine the optimum site for effective pain reduction (patients 1 and 2) or epileptic foci localization (patient 3).

Behavioral Tasks

Patients executed the tasks in an electromagnetically shield room approximately one week after electrode implantation. All patients were seated upright on a chair at a table and were asked to perform the tasks using their left hands. Patient 1 repositioned three blocks around a 25 cm × 25 cm square one by one and in a clockwise fashion (green arrows in Figure 1). He moved his hand to the first block (a rectangular parallelepiped in Figure 1), grasped it, carried it to the vacant corner of the square, and released it. Next, he moved the second block (a cube) to the corner vacated by the rectangular parallelepiped. Finally, he moved the third block (a cylinder) to the corner vacated by the cube. When all objects had been moved to the next corner once, a cycle of hand motion was completed. Patient 1 regularly repeated nine cycles in session 1 and eleven cycles in session 2. Patient 2 also carried the three blocks to vacant corners of the square, but he randomly chose one block among the three to move. Patient 2 performed similar arm movements 19 and 20 times for sessions 1 and 2, respectively. Patient 3 chose one of three blocks and placed it at an arbitrary position on the table. He performed 18, 31, and 24 movements in sessions 1, 2 and 3, respectively. We instructed patients to perform the tasks at their own pace. Each session started just after an audio cue, delivered through a speaker controlled with a MATLAB R2007b (Mathworks, Inc., Natick, MA, USA) script, and

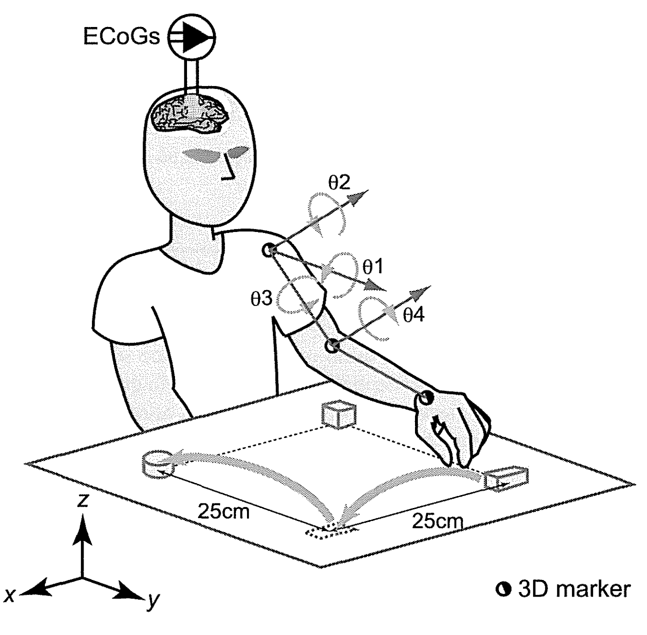

Figure 1. Behavioral tasks. Patient 1 repositioned three blocks one by one and clockwise (green arrows) at the corners of a 25 cm × 25 cm square. ECoG signals were obtained with planar-surface platinum grid electrodes placed on the right sensorimotor cortex. Half-closed circles on the left shoulder, elbow, and wrist joints represent three-dimensional markers for the motion capture system. The angles q1, q2, q3, and q4 are defined as an abduction/adduction angle, a flexion/extension angle, an external/internal rotation at the left shoulder joint, and a flexion/extension angle at the left elbow joint, respectively. When he lowered his arm toward the -*z* direction and turned his palm to the *y* direction with the elbow extended, q1, q2, and q3 were all zero, and q4 was π radians.
doi:10.1371/journal.pone.0072085.g001

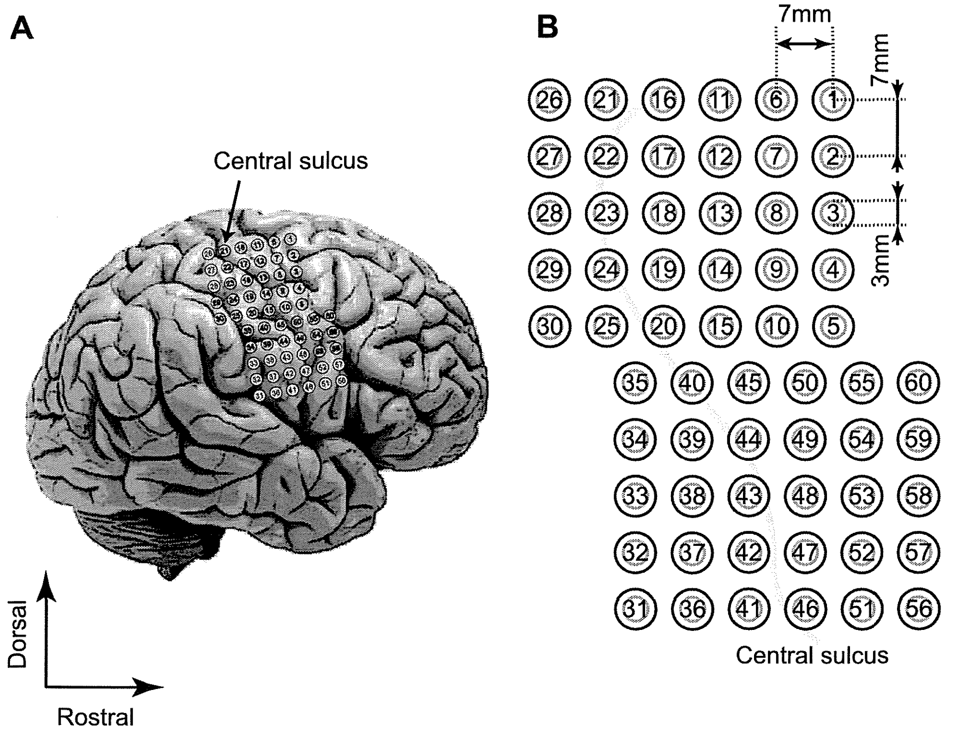

Figure 2. Electrodes placed on the sensorimotor cortex of patient 1. (A) Positions of the electrodes (circles). (B) Two 5 × 6 electrode arrays were placed on the right hemisphere, covering the sensorimotor cortex. Yellow lines depict the right central sulcus.
doi:10.1371/journal.pone.0072085.g002

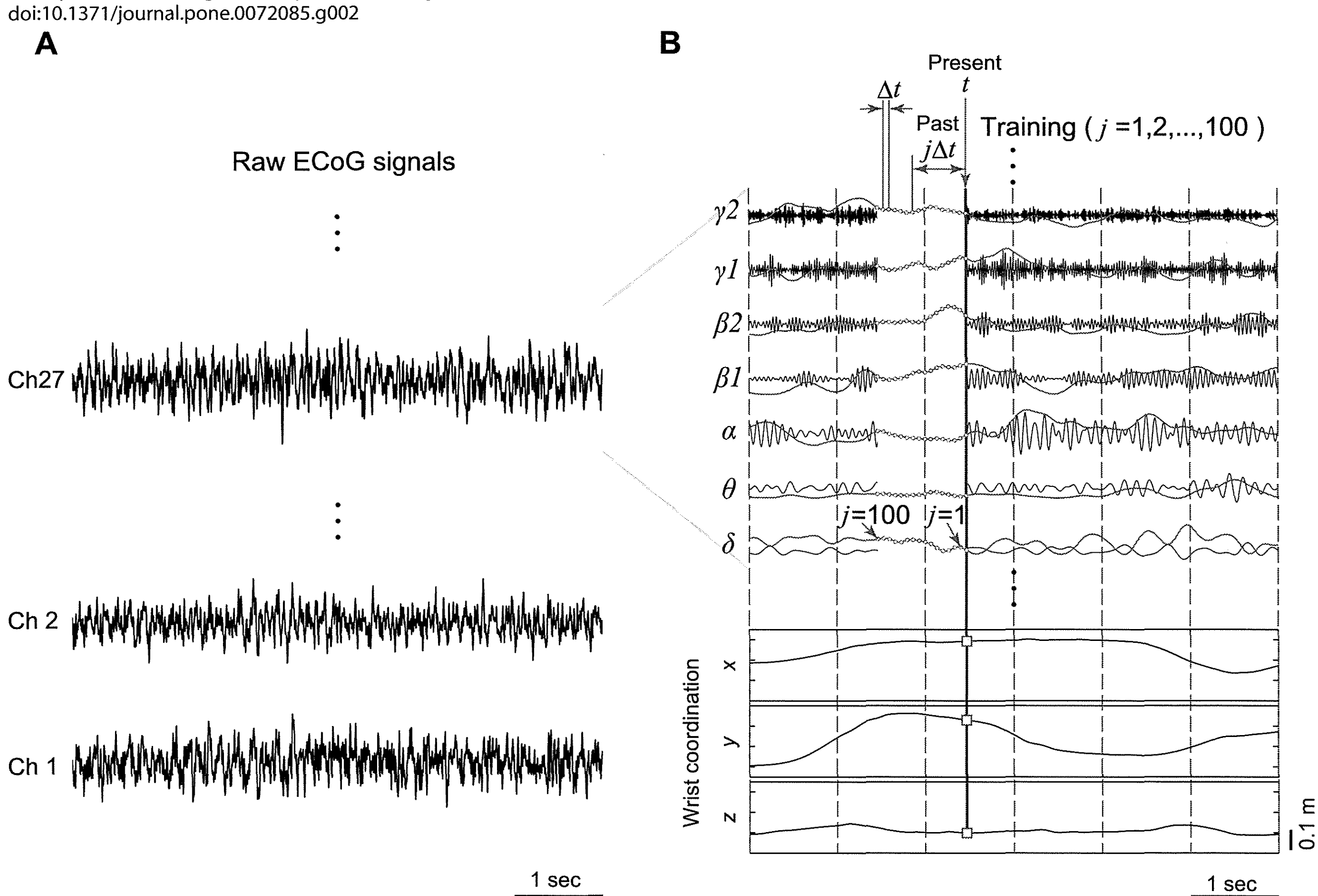

Figure 3. ECoG signal processing and decoding method. (A) Raw ECoG signals from channels 1, 2, and 27 are shown as typical examples. (B) The ECoG signal of channel 27 was divided into seven frequency components ($\delta, \theta, \ldots, \gamma$ 2) with bandpass filters (black lines). These seven filtered signals were digitally rectified, smoothed with a low-pass filter, and down-sampled to 100 Hz. The band-passed ECoG signals were then *z*-score normalized (red lines). The linear relationship between the past 1 s of normalized ECoG (light-blue area; $t \sim t\text{-}j\Delta t, j = 1, 2, \ldots, 100, \Delta t = 0.01$ s, i.e., 100 sampling points) and a coordinate *x*, *y*, or *z* at the present *t* (tiny yellow boxes) was determined using sparse linear regression. Once weight coefficients were obtained through training, construction of the decoder was complete.
doi:10.1371/journal.pone.0072085.g003

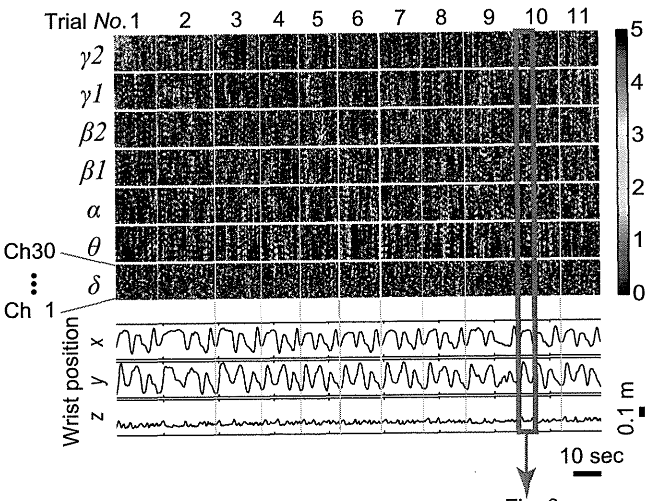

Figure 4. Color-map of the normalized ECoG signals and coordinates at the left wrist joint. Signals were obtained from channels 1~30 in session 2 of patient 1(channels 31~60 are not shown). This session includes 11 cycles. We treated each cycle as an independent trial.Start and end points were respectively defined as the instances where tangential velocity of the arm exceeded or fell below 5% of maximum velocity. Unused sampling points are colored yellow (yellow vertical lines). Precise wave forms of *z*-score on channel 27 inside of a red rectangle were already displayed in detail in Figure 3.
doi:10.1371/journal.pone.0072085.g004

continued for 180 seconds. We excluded 20 trials in which patient 2 moved more than 20 cm sagittally because his torso swung forward and backward during the tasks. The abovementioned tasks included several actions, i.e., reaching, grasping, carrying and releasing, which are basic and indispensable actions for daily life.

ECoG Signals and Motion Recordings

Patients 1 and 2 were implanted with two 5×6 electrode arrays, and patient 3 was implanted with a 3×5 array. The planar-surface platinum grid electrodes had a diameter of 3 mm and an inter-electrode distance of 7 mm, as shown in Figure 2. The number of electrodes was 60 for patients 1 and 2, and 15 for patient 3. ECoG signals were recorded inside an electromagnetically shielded room with a 128-channel digital EEG system (EEG 2000; Nihon Koden Corporation, Tokyo, Japan) set at a sampling rate of 1000 Hz. All electrodes were referenced to a scalp electrode on the nasion of each patient. Figure 2A shows electrodes placed on the cortex of patient 1.

3D arm motions were recorded at a sampling rate of 100 Hz with an optical motion capture system (Eagle Digital System; Motion Analysis Corporation, Santa Rosa, CA) using reflecting 3D markers shaped in 6 mm-diameter spheroids to identify the left shoulder, left elbow, and left wrist joint positions (Figure 1). The frame lengths of images available for leave-one-out cross-validation (LOO-CV) were as follows: 180 seconds for each session by patient 1, 120 seconds for each session by patient 2, and 90, 180 and 120 seconds for sessions 1, 2, and 3 by patient 3, respectively. Frame lengths differed between patients and sessions since the 3D markers occasionally went out of the field of view or were occluded by the patient's body. The start of ECoG and motion capture recordings was time-locked to the cue signal.

ECoG Signal Processing

ECoG signals were pre-processed with our previously proposed method [44]. Firstly, the signal data sampled at 1000 Hz were re-referenced with a common average reference (CAR) and divided into seven frequency bands (δ : ~4 Hz, θ : 4~8 Hz, α: 8~14 Hz, β 1:14~20 Hz, β 2:20~30 Hz, γ 1:30~50 Hz, and γ 2:50~90 Hz) using fourth-order bandpass Butterworth filters (Figure 3). Secondly, these band-passed signals were digitally rectified and smoothed with a second-order low-pass filter (cut-off frequency: 2.2 Hz), which changed high oscillations into low frequency features. Thirdly, the signals were down sampled to 100 Hz, i.e., the sampling rate of the motion capture recordings. Finally, the obtained signals $x_i(t)$ ($i = 1, 2, \ldots, n$ 7) at time t were normalized to the standard z-score $z_i(t)$ as follows (red lines in Figure 3B).

$$z_i(t) = \frac{x_i(t) - \mu_i}{\sigma_i} \quad (i = 1, 2, \ldots, n \times 7) \tag{1}$$

where μ_i, σ_i and n denote the mean value of $x_i(t)$, the standard deviation of $x_i(t)$, and the number of ECoG channels, respectively. These z-scores calculated from ECoG signals were utilized as training data to construct a decoder.

Decoding Method

The value of an angle or a coordinate $Y_p(t)$ at a present time t was predicted with the following linear equation:

$$Y_p(t) = \sum_{i=1}^{n \times 7} \sum_{j=1}^{m} w_{ij} z_i(t - j\Delta t) + w_0 \tag{2}$$

where Δt and m denote time-step and the number of consecutive sampling points before the present time t used to predict Y_p at t, respectively. In this study, we assigned 100 points and 0.01 seconds to m and Δt, respectively. w_0 and w_{ij} are, respectively, a bias term and a weight coefficient to the i-th filtered ECoG signal z_i at time t-$j\Delta t$ (Figure 3B). We applied a Bayesian algorithm called sparse linear regression [44,46–49] to determine values of the weights w_{ij}.

Each session was segmented into 9~31 trials. Figure 4 shows z-scores and coordinates x, y and z at the wrist joint in session 2 of patient 1. In this example, the session was divided into 11 trials. We defined the starting point of each trial as the instance when tangential velocity at the elbow joint exceeded 5% of the maximum velocity in the trial. The end point of each trial was decided in a similar manner, i.e., the instance when tangential velocity decreased to less than 5% of maximum. In Figure 4, unused data between the k-th ending point and the k+1-th starting point are colored over with yellow (yellow vertical lines).

We verified the validity of our method using LOO-CV. Firstly, a decoder was constructed using filtered ECoG signals and actual arm position or actual joint angle in all trials except the k-th trial, which was used as test data. The weight coefficients w_{ij} were obtained from this training. Iterations of the sparse linear regression were terminated just before over-training. Secondly, an arm trajectory Y_p in the k-th trial was predicted with the decoder. Pearson's correlation coefficient (CC) and the normalized root-mean-square error (nRMSE) were obtained by comparing Y_p and Y_{act} of the k-th test trial. Thirdly, the abovementioned training and testing phases were repeatedly executed using different trials for k (Figure 4, $k = 1, 2, \ldots, 11$). Finally the CC and nRMSE values were averaged across all trials.

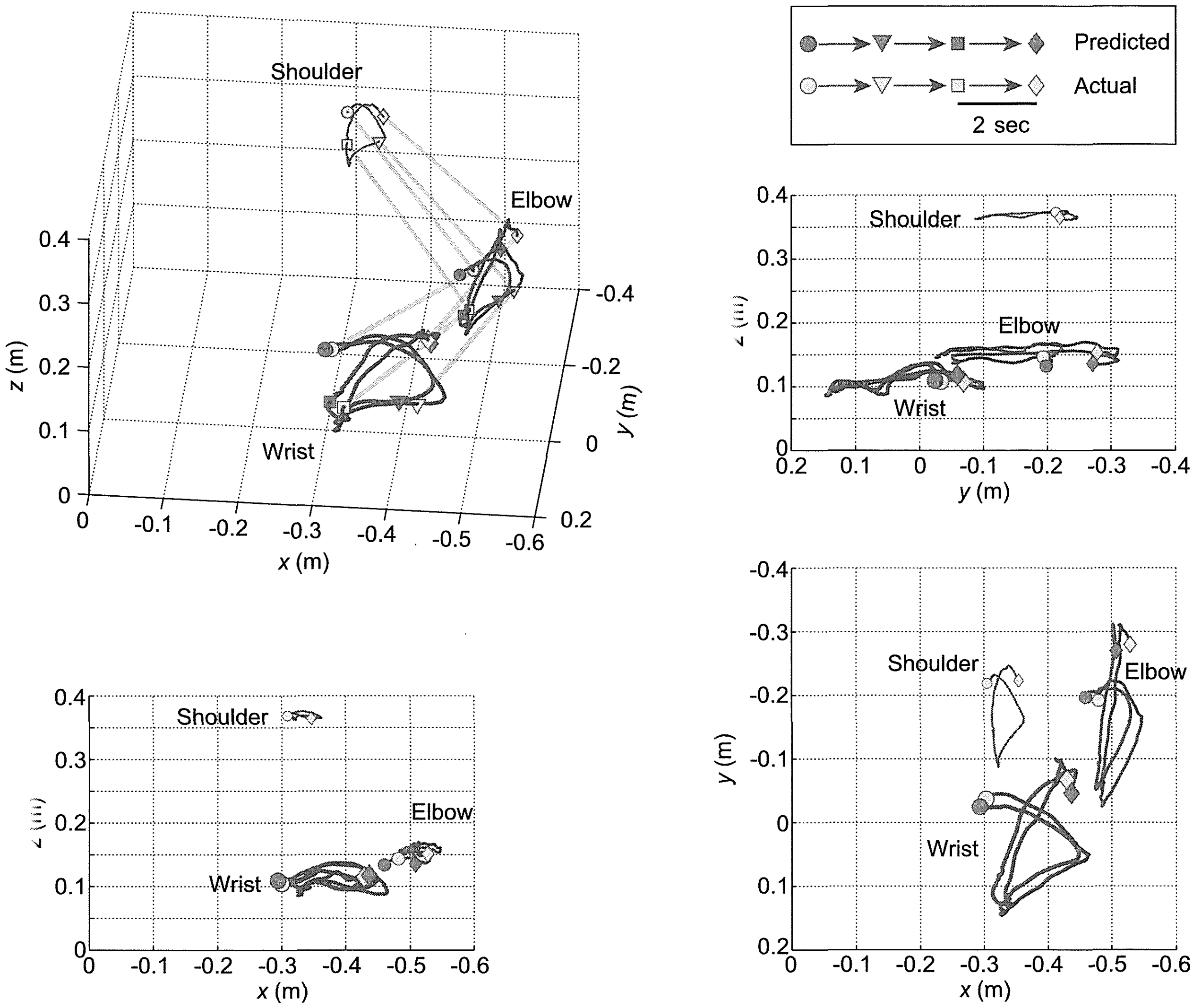

Figure 5. Examples of the predicted (red lines) and actual 3D trajectories (blue lines). A part of the 10th trial (6 s) in session 2 of patient 1 is shown (see Video S1). Markers (circles, triangles, squares, and diamonds) represent 2 s time intervals. Circles and diamonds indicate the earliest and the latest positions, respectively. The red trajectories were computed using predicted data q1~q4 and patient 1's actual arm length. The timings (positions of the markers) and trajectory curves of the predicted data were similar to those of the actual data.
doi:10.1371/journal.pone.0072085.g005

Results

Reconstruction of Angles and Positions

Movement duration average and standard deviations across 20 trials for patient 1 was 17.17 ± 2.76 s, indicating that his motion in each trial was non-uniform (see Fig. S1). Figure 5 is an example of the comparison between predicted (red lines) and actual 3D trajectories (blue lines) for six seconds in the 10th trial of session 2 by patient 1. The red lines were drawn using inferred joint angles q1~ q4 and the patient's arm length. Figure 6 shows predicted joint angles (red lines in the left column) and joint positions (red lines in the center and right columns) in comparison with actual measurements (blue lines) in the 10th trial of session 2 as typical plots by patient 1 (Figure 4). In this trial, it took 15.1 s to move all three blocks to the next open corners of the square. Most blue lines have curvatures with three peaks representing the three block moving tasks. The timings of the peaks differed between q2 and q3 indicated by green arrows. The predicted red lines fit the peaks at various timings, even though the ECoG signals utilized for the prediction were common between q2 and q3. The traces for q1, z at the elbow, and z at the wrist have narrow variation ranges and many peaks, in contrast to those of the other joint angles/coordinates. The ranges of CC and nRMSE for joint angles (left column in Figure 6) were 0.57~0.88 and 0.13~0.40, respectively. The flexion/extension angle q2 at the left shoulder showed the best result. CC and nRMSE for joint coordinates (middle and right columns) were 0.48~0.82 and 0.16~0.30, respectively. The y coordinate values at the elbow were relatively greater than those of the other coordinates. Both q2 and y at elbow showed wider ranges of variation than the others.

Average CC and average nRMSE of the three patients are summarized in Figure 7. The best average CC and nRMSE among joint angles were 0.71 ± 0.026 and 0.23 ± 0.010 (mean ± SEM), respectively, corresponding to angle q2 for patient 1. The

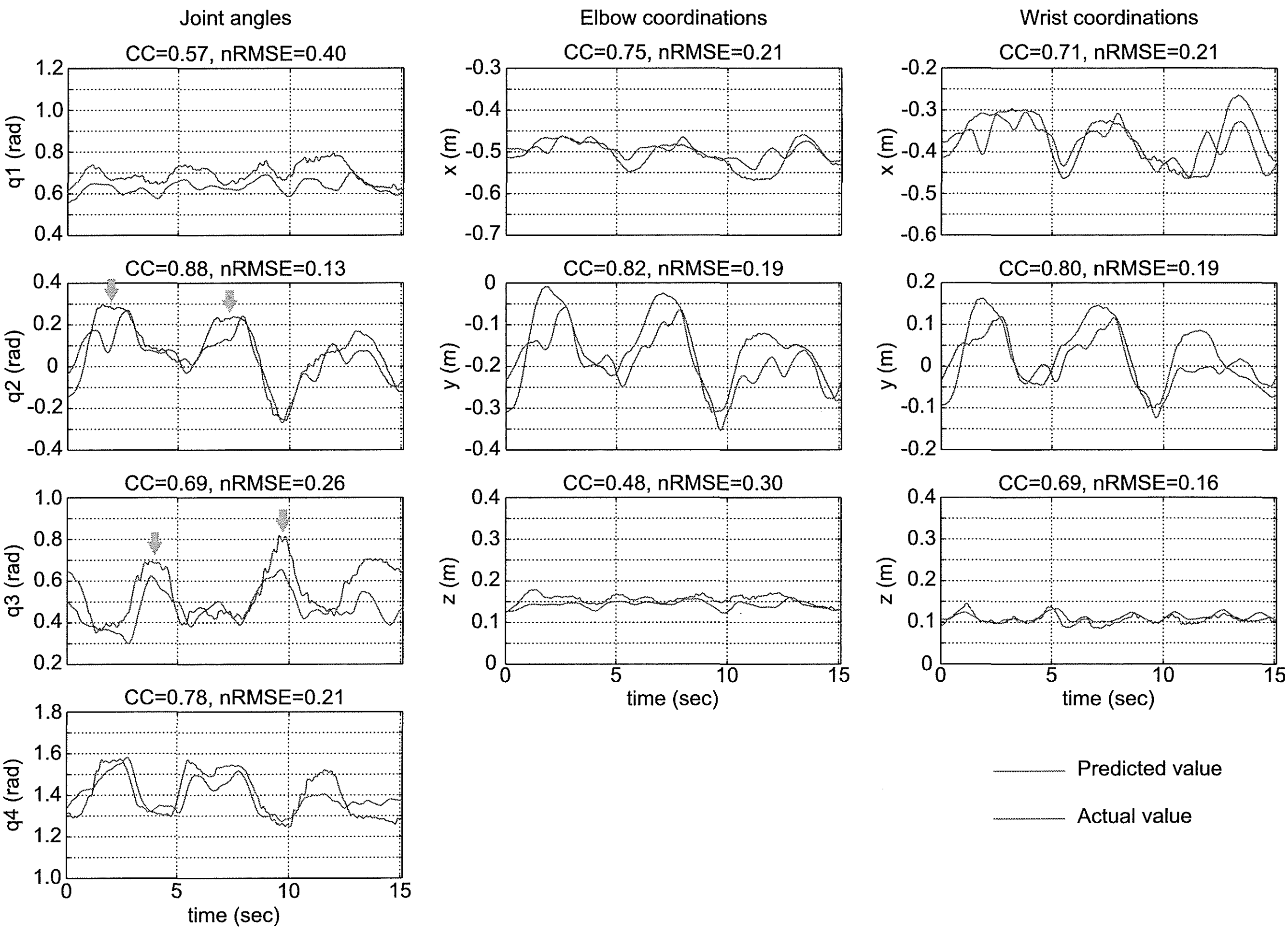

Figure 6. Examples of predicted joint angles and positions in time series. Blue lines are actual recoded joint angles (left column), and actual positions at the left elbow (center column) and left wrist joint (right column) in the 10th trial shown in Figure 3 and Figure 4. The joint angles and coordinates predicted with sparse linear regression are plotted in red. The Pearson's correlation coefficient (CC) and the normalized root-mean-square error (nRMSE) are shown at the top of each graph.
doi:10.1371/journal.pone.0072085.g006

best average CC and nRMSE among joint coordinates were 0.73 ± 0.022 and 0.18 ± 0.0071, respectively, corresponding to the z coordinate of the left wrist for patient 1.

To judge whether performance of the proposed method differed significantly between patients, a two-way ANOVA with Tukey's multiple-comparison test was conducted to analyze the effects of two factors (patients and joint angles; patients and joint coordination). The 2-way interaction did not show any significance. Significant differences were observed among the patients (joint angle: $F_{2,\ 436}=82.46$, $p<0.001$; coordination: $F_{2,\ 654}=117.56$, $p<0.001$), whereas significant differences were not observed among joint angles and joint coordination. The CC values of both patients 1 and 2 were significantly higher than those of patient 3. The nRMSE values for patient 3 were also significantly higher than those of the other patients (joint angle: $F_{2,\ 436}=10.42$, $p<0.05$; coordination: $F_{2,\ 654}=41.14$, $p<0.01$). This may be interpreted such that the proposed method is more suitable for patients 1 and 2 than for patient 3.

Frequency Components Contributing to Reconstruction of Arm Trajectory

3D hand trajectories were predicted using each sensorimotor rhythm, one by one. The results averaged across 20 trials for patient 1 are shown in Figure 8. A two-way ANOVA was employed to judge two effects (seven sensorimotor frequency bands and four joint angles or six coordinations). Among the 2-way interactions, only elbow coordination showed significance (joint angle: $F_{18,\ 532}=1.07$, $p=0.38$; elbow coordination: $F_{12,\ 399}=1.86$, $p=0.04$; wrist coordination: $F_{12,\ 399}=1.4$, $p=0.16$). Significant differences were observed among the sensorimotor frequency bands (joint angle: $F_{6,\ 532}=27.26$, $p<0.001$; elbow coordination: $F_{6,\ 399}=33.67$, $p<0.001$; wrist coordination: $F_{6,\ 399}=43.58$, $p<0.001$), as shown in figure 8. The CC values of the δ and γ2 bands were significantly higher than those of the other bands.

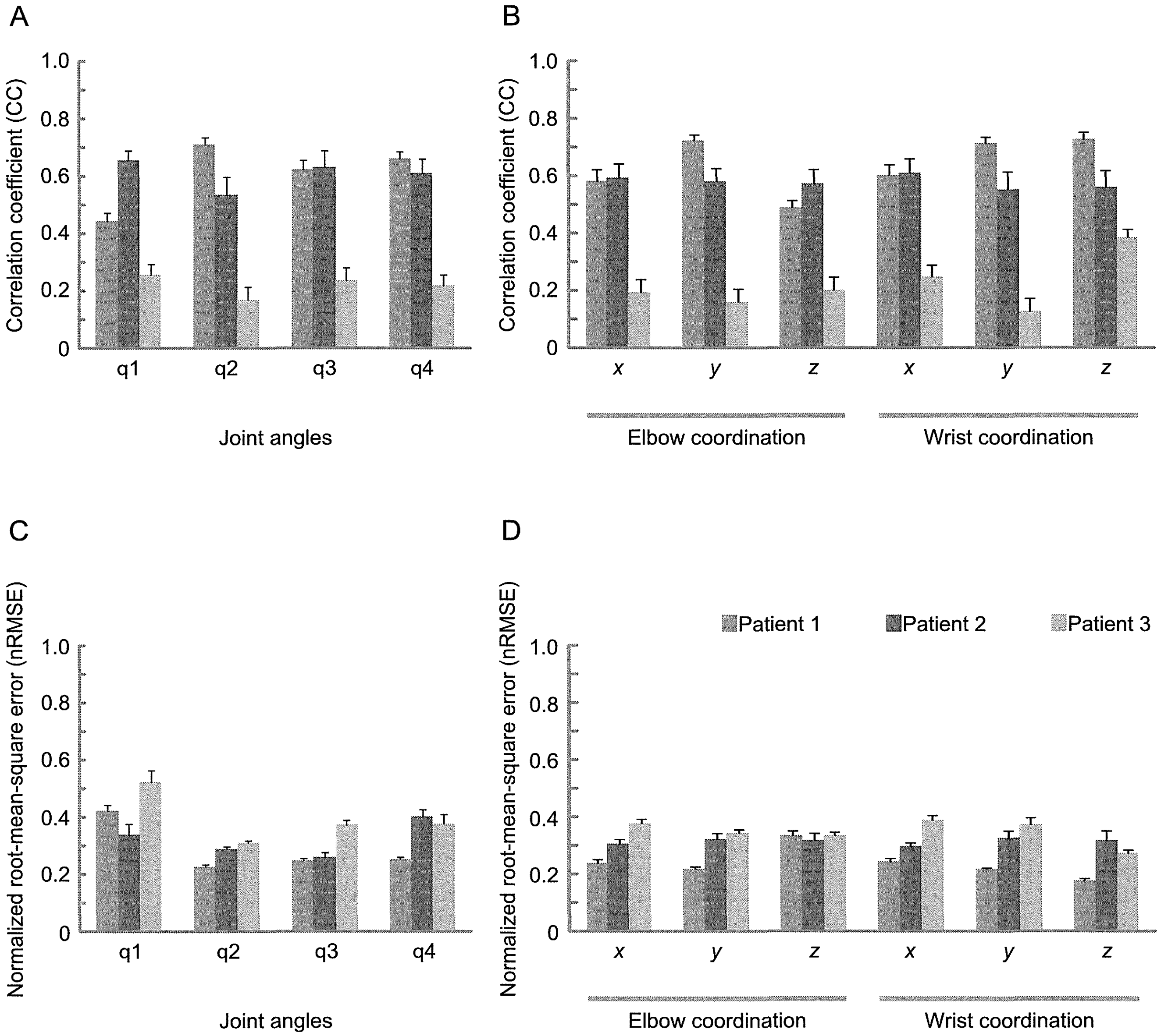

Figure 7. Prediction results for all patients. Averaged correlation coefficients (CC) for joint angle (A) and *x*, *y*, *z* coordination (B), and the normalized root-mean-square error (nRMSE) for joint angles (C) and *x*, *y*, *z* coordination (D) were obtained using LOO-CV on 20, 19 and 73 trials for patients 1, 2, and 3 (blue, red, and green bars), respectively.
doi:10.1371/journal.pone.0072085.g007

Discussion

We predicted 3D arm trajectory in humans based on ECoG signals divided into seven frequency bands using a sparse linear regression method. Although two-dimensional (2D) cursor trajectories on a display have been precisely predicted using ECoG signals obtained from patients in several studies [35,37–38], to the best of our knowledge, inference of 3D trajectory for the human arm using ECoG has not been previously presented.

We inferred both joint angles (q1~ q4) and joint positions (*x*, *y* and *z*) to reconstruct 3D trajectory and obtained acceptable prediction accuracies in both cases. Our average CC and nRMSE were 0.44~0.73 and 0.18~0.42, respectively, excluding patient 3. In the previous studies on 2D cursor trajectories with humans, average CC were approximately 0.22~0.71 for Schalk et al. (2007) (with the average across positions and velocities for the best participant being 0.62) [35], 0.3~0.6 for Pistohl et al. (2008) [37], and 0.52~0.87 for Gunduz et al. (2009) [38]. Kubanek et al. (2009), who predicted individual finger flexions, showed an average CC of 0.23 (little finger) ~ 0.75 (thumb) (CC averaged across all fingers and participants was 0.52) [41]. Our results were not inferior to the aforementioned studies, especially considering the higher dimensionality of trajectory data.

The prediction accuracy for patient 3 was significantly worse than that of the other patients. His average CC and nRMSE were 0.13~0.38 and 0.28~0.52, respectively. We suggest the following as possible causes for this result: (1) ECoG signal quality; There were obvious disturbances or noise in his ECoG signals which

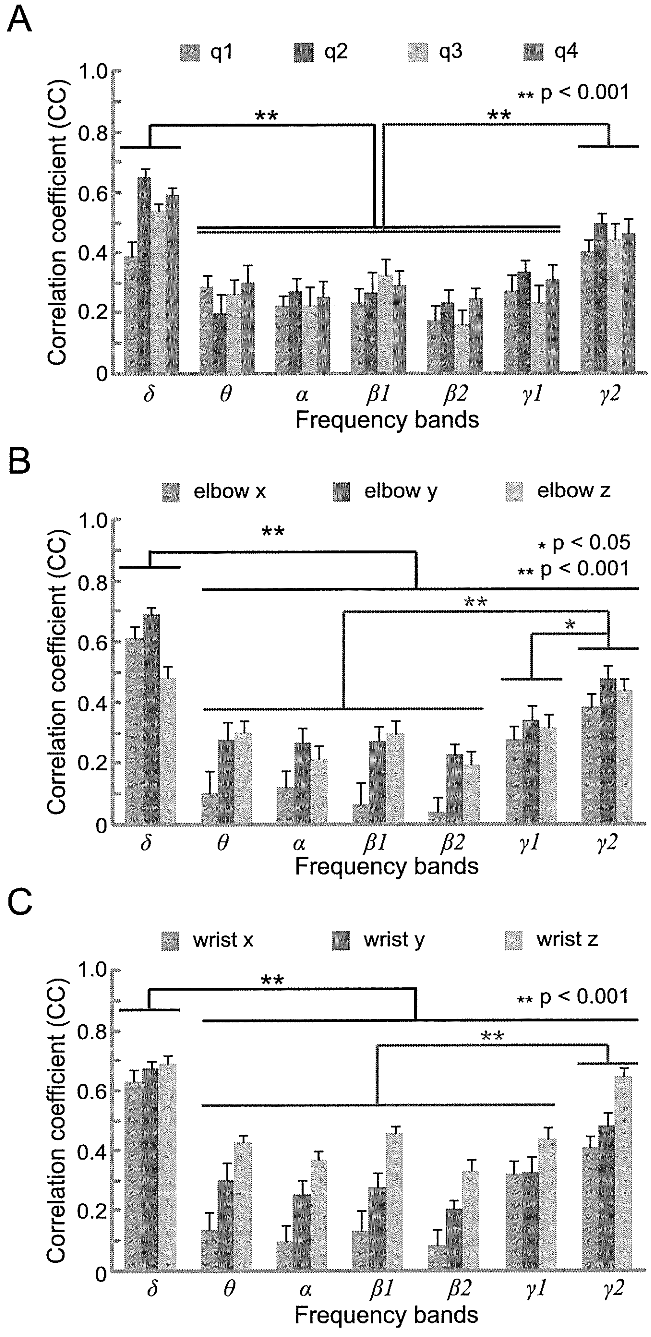

Figure 8. Contribution of each frequency band for trajectory prediction. Each panel (A: joint angles; B: *xyz* coordinates of the elbow; C: *xyz* coordinates of the wrist) shows the results of prediction using each sensorimotor rhythm, one by one. Noteworthy significant differences between CC values of frequency bands are marked with * ($p<0.05$) and ** ($p<0.001$). Other significance comparisons are omitted for visualization purposes.
doi:10.1371/journal.pone.0072085.g008

could be discerned through visual inspection. The baselines of his ECoG signals also randomly and widely fluctuated. (2) Electrode number; Patient 3 had only 15 electrodes placed around his central sulcus, whereas the other patients had 60 electrodes. (3) Pathology; Patient 3 had epilepsy while the others did not. (4) Task properties; He was allowed to place the blocks at arbitrary places on the table. He decided their positions impromptu, in contrast to the other participants who placed their blocks at fixed positions. We suggest that much more training data are necessary for the prediction of motions involving various postures such as those in the data of patient 3.

Joint angle q1 could not be predicted precisely, in contrast to q2~q4 (Figure 7A and 6C). The range of abduction/adduction for q1 was the narrowest among all angles, as shown in the left column of Figure 6. We presume that it was difficult to extract the faint component correlating with this small fluctuation from ECoG as a summation of various signals.

The high frequency band γ2 (50~90 Hz) had relatively high CC values (Figure 8). Several papers also reported that high frequency bands of ECoG were important for prediction, such as 40~80 Hz for cursor trajectory prediction in humans [37], 80~150 Hz for the classification of human hand movements [31], 40~90 Hz for 3D hand trajectory prediction in monkeys [43], and 50~90 Hz for EMG prediction in monkeys [44]. The low frequency band δ (~4 Hz) had the highest values among the seven bands in this study. This was also supported by previous works [32,37] which reported that the low frequency band ECoG (2~6 Hz; with band-pass filter) and low frequency component (LFC) (<5 Hz; with Savitzky-Golay smoothing filter) were important for classifying different grasp types [32].

We verified that 3D arm trajectories in patients of different pathology could be predicted with our proposed method using a sparse linear regression. We foresee this method contributing to further studies and further improvements in neuroprostheses and neurorehabilitation.

Supporting Information

Figure S1 Actual position at the wrist joint for patient 1. Coordinates x, y, and z of all 20 trials are shown. Motion of patient 1 was non-uniform, with duration and timing differing between trials.
(EPS)

Video S1 Examples of the predicted arm positions of patient 1. Blue and red lines are actual and predicted arm positions in the 10th trial of session 2, respectively.
(MOV)

Acknowledgments

We thank the participants for their commitment and effort for this study. We thank the contribution and support from clinicians and researchers at the Osaka University Hospital. We thank also C. S. DaSalla for proofreading the manuscript.

Author Contributions

Conceived and designed the experiments: T. Yanagisawa MH T. Yoshimine. Performed the experiments: T. Yanagisawa MH RF T. Yoshimine. Analyzed the data: YN DS. Contributed reagents/materials/analysis tools: YN DS CC HK NY YK. Wrote the paper: YN T. Yanagisawa DS.

References

1. Wolpaw JR, McFarland DJ, Neat GW, Forneris CA (1991) An EEG-based brain-computer interface for cursor control. Electroencephalogr Clin Neurophysiol 78: 252–259.
2. Wolpaw JR, McFarland DJ (2004) Control of a two-dimensional movement signal by a noninvasive brain-computer interface in humans. Proc Natl Acad Sci U S A 101: 17849–17854.
3. Blankertz B, Dornhege G, Schafer C, Krepki R, Kohlmorgen J, et al. (2003) Boosting bit rates and error detection for the classification of fast-paced motor commands based on single-trial EEG analysis. IEEE Trans Neural Syst Rehabil Eng 11: 127–131.
4. Blankertz B, Dornhege G, Krauledat M, Muller KR, Kunzmann V, et al. (2006) The Berlin Brain-Computer Interface: EEG-based communication without subject training. IEEE Trans Neural Syst Rehabil Eng 14: 147–152.
5. Waldert S, Preissl H, Demandt E, Braun C, Birbaumer N, et al. (2008) Hand movement direction decoded from MEG and EEG. J Neurosci 28: 1000–1008.
6. Birbaumer N, Ghanayim N, Hinterberger T, Iversen I, Kotchoubey B, et al. (1999) A spelling device for the paralysed. Nature 398: 297–298.
7. Pfurtscheller G, Neuper C (1994) Event-related synchronization of mu rhythm in the EEG over the cortical hand area in man. Neurosci Lett 174: 93–96.
8. Birbaumer N, Cohen LG (2007) Brain-computer interfaces: communication and restoration of movement in paralysis. J Physiol 579: 621–636.
9. Daly JJ, Wolpaw JR (2008) Brain-computer interfaces in neurological rehabilitation. Lancet Neurol 7: 1032–1043.
10. Buch E, Weber C, Cohen LG, Braun C, Dimyan MA, et al. (2008) Think to move: a neuromagnetic brain-computer interface (BCI) system for chronic stroke. Stroke 39: 910–917.
11. Broetz D, Braun C, Weber C, Soekadar SR, Caria A, et al. (2010) Combination of brain-computer interface training and goal-directed physical therapy in chronic stroke: a case report. Neurorehabil Neural Repair 24: 674–679.
12. Soekadar SR, Witkowski M, Mellinger J, Ramos A, Birbaumer N, et al. (2011) ERD-based online brain-machine interfaces (BMI) in the context of neurorehabilitation: optimizing BMI learning and performance. IEEE Trans Neural Syst Rehabil Eng 19: 542–549.
13. Shindo K, Kawashima K, Ushiba J, Ota N, Ito M, et al. (2011) Effects of neurofeedback training with an electroencephalogram-based brain-computer interface for hand paralysis in patients with chronic stroke: a preliminary case series study. J Rehabil Med 43: 951–957.
14. Mehring C, Rickert J, Vaadia E, Cardosa de Oliveira S, Aertsen A, et al. (2003) Inference of hand movements from local field potentials in monkey motor cortex. Nat Neurosci 6: 1253–1254.
15. Koike Y, Hirose H, Sakurai Y, Iijima T (2006) Prediction of arm trajectory from a small number of neuron activities in the primary motor cortex. Neurosci Res 55: 146–153.
16. Wu W, Gao Y, Bienenstock E, Donoghue JP, Black MJ (2006) Bayesian population decoding of motor cortical activity using a Kalman filter. Neural Comput 18: 80–118.
17. Stark E, Abeles M (2007) Predicting movement from multiunit activity. J Neurosci 27: 8387–8394.
18. Serruya MD, Hatsopoulos NG, Paninski L, Fellows MR, Donoghue JP (2002) Instant neural control of a movement signal. Nature 416: 141–142.
19. Chapin JK, Moxon KA, Markowitz RS, Nicolelis MA (1999) Real-time control of a robot arm using simultaneously recorded neurons in the motor cortex. Nat Neurosci 2: 664–670.
20. Taylor DM, Tillery SI, Schwartz AB (2002) Direct cortical control of 3D neuroprosthetic devices. Science 296: 1829–1832.
21. Carmena JM, Lebedev MA, Crist RE, O'Doherty JE, Santucci DM, et al. (2003) Learning to control a brain-machine interface for reaching and grasping by primates. PLoS Biol 1: E42.
22. Velliste M, Perel S, Spalding MC, Whitford AS, Schwartz AB (2008) Cortical control of a prosthetic arm for self-feeding. Nature 453: 1098–1101.
23. Moritz CT, Perlmutter SI, Fetz EE (2008) Direct control of paralysed muscles by cortical neurons. Nature 456: 639–642.
24. Hochberg LR, Serruya MD, Friehs GM, Mukand JA, Saleh M, et al. (2006) Neuronal ensemble control of prosthetic devices by a human with tetraplegia. Nature 442: 164–171.
25. Kennedy PR, Kirby MT, Moore MM, King B, Mallory A (2004) Computer control using human intracortical local field potentials. IEEE Trans Neural Syst Rehabil Eng 12: 339–344.
26. Polikov VS, Tresco PA, Reichert WM (2005) Response of brain tissue to chronically implanted neural electrodes. J Neurosci Methods 148: 1–18.
27. Leuthardt EC, Schalk G, Wolpaw JR, Ojemann JG, Moran DW (2004) A brain-computer interface using electrocorticographic signals in humans. J Neural Eng 1: 63–71.
28. Chin CM, Popovic MR, Thrasher A, Cameron T, Lozano A, et al. (2007) Identification of arm movements using correlation of electrocorticographic spectral components and kinematic recordings. J Neural Eng 4: 146–158.
29. Ball T, Schulze-Bonhage A, Aertsen A, Mehring C (2009) Differential representation of arm movement direction in relation to cortical anatomy and function. J Neural Eng 6: 016006.
30. Yanagisawa T, Hirata M, Saitoh Y, Kato A, Shibuya D, et al. (2009) Neural decoding using gyral and intrasulcal electrocorticograms. Neuroimage 45: 1099–1106.
31. Yanagisawa T, Hirata M, Saitoh Y, Kishima H, Matsushita K, et al. (2012) Electrocorticographic control of a prosthetic arm in paralyzed patients. Ann Neurol 71: 353–361.
32. Pistohl T, Schulze-Bonhage A, Aertsen A, Mehring C, Ball T (2012) Decoding natural grasp types from human ECoG. Neuroimage 59: 248–260.
33. Chestek CA, Gilja V, Blabe CH, Foster BL, Shenoy KV, et al. (2013) Hand posture classification using electrocorticography signals in the gamma band over human sensorimotor brain areas. J Neural Eng 10: 026002.
34. Leuthardt EC, Miller KJ, Schalk G, Rao RP, Ojemann JG (2006) Electrocorticography-based brain computer interface–the Seattle experience. IEEE Trans Neural Syst Rehabil Eng 14: 194–198.
35. Schalk G, Kubanek J, Miller KJ, Anderson NR, Leuthardt EC, et al. (2007) Decoding two-dimensional movement trajectories using electrocorticographic signals in humans. J Neural Eng 4: 264–275.
36. Schalk G, Miller KJ, Anderson NR, Wilson JA, Smyth MD, et al. (2008) Two-dimensional movement control using electrocorticographic signals in humans. J Neural Eng 5: 75–84.
37. Pistohl T, Ball T, Schulze-Bonhage A, Aertsen A, Mehring C (2008) Prediction of arm movement trajectories from ECoG-recordings in humans. J Neurosci Methods 167: 105–114.
38. Gunduz A, Sanchez JC, Carney PR, Principe JC (2009) Mapping broadband electrocorticographic recordings to two-dimensional hand trajectories in humans Motor control features. Neural Netw 22: 1257–1270.
39. Leuthardt EC, Gaona C, Sharma M, Szrama N, Roland J, et al. (2011) Using the electrocorticographic speech network to control a brain-computer interface in humans. J Neural Eng 8: 036004.
40. Wang W, Collinger JL, Degenhart AD, Tyler-Kabara EC, Schwartz AB, et al. (2013) An Electrocorticographic Brain Interface in an Individual with Tetraplegia. PLoS ONE 8: e55344.
41. Kubanek J, Miller KJ, Ojemann JG, Wolpaw JR, Schalk G (2009) Decoding flexion of individual fingers using electrocorticographic signals in humans. J Neural Eng 6: 066001.
42. Chao ZC, Nagasaka Y, Fujii N (2010) Long-term asynchronous decoding of arm motion using electrocorticographic signals in monkeys. Front Neuroeng 3: 3.
43. Shimoda K, Nagasaka Y, Chao ZC, Fujii N (2012) Decoding continuous three-dimensional hand trajectories from epidural electrocorticographic signals in Japanese macaques. J Neural Eng 9: 036015.
44. Shin D, Watanabe H, Kambara H, Nambu A, Isa T, et al. (2012) Prediction of muscle activities from electrocorticograms in primary motor cortex of primates. PLoS One 7: e47992.
45. Watanabe H, Sato MA, Suzuki T, Nambu A, Nishimura Y, et al. (2012) Reconstruction of movement-related intracortical activity from micro-electrocorticogram array signals in monkey primary motor cortex. J Neural Eng 9: 036006.
46. Sato M (2001) Online model selection based on the variational bayes. Neural Computation 13: 1649–1681.
47. Ting JA, D'Souza A, Yamamoto K, Yoshioka T, Hoffman D, et al. (2008) Variational Bayesian least squares: an application to brain-machine interface data. Neural Netw 21: 1112–1131.
48. Nambu I, Osu R, Sato MA, Ando S, Kawato M, et al. (2009) Single-trial reconstruction of finger-pinch forces from human motor-cortical activation measured by near-infrared spectroscopy (NIRS). Neuroimage 47: 628–637.
49. Yoshimura N, DaSalla CS, Hanakawa T, Sato MA, Koike Y (2012) Reconstruction of flexor and extensor muscle activities from electroencephalography cortical currents. Neuroimage 59: 1324–1337.

35th Annual International Conference of the IEEE EMBS
Osaka, Japan, 3 - 7 July, 2013

Development of an Implantable Wireless ECoG 128ch Recording Device for Clinical Brain Machine Interface

Kojiro Matsushita, Masayuki Hirata, Takafumi Suzuki, Hiroshi Ando, Yuki Ota, Fumihiro Sato, Shyne Morris, Takeshi Yoshida, Hidetoshi Matsuki, Toshiki Yoshimine

Abstract— **Brain Machine Interface (BMI) is a system that assumes user's intention by analyzing user's brain activities and control devices with the assumed intention. It is considered as one of prospective tools to enhance paralyzed patients' quality of life. In our group, we especially focus on ECoG (electro-corti-gram)-BMI, which requires surgery to place electrodes on the cortex. We try to implant all the devices within the patient's head and abdomen and to transmit the data and power wirelessly. Our device consists of 5 parts: (1) High-density multi-electrodes with a 3D shaped sheet fitting to the individual brain surface to effectively record the ECoG signals; (2) A small circuit board with two integrated circuit chips functioning 128 [ch] analogue amplifiers and A/D converters for ECoG signals; (3) A Wifi data communication & control circuit with the target PC; (4) A non-contact power supply transmitting electrical power minimum 400[mW] to the device 20[mm] away. We developed those devices, integrated them, and, investigated the performance.**

I. INTRODUCTION

Electrocorticogram (ECoG) indicates a biological electrical activity, which is recorded with the electrodes directly placed on brain surface. It characterizes higher spatial resolution (better signal-to-noise ratio) compared to electroencephalograms (EEG) [1], and provide lower risk due to a less-invasive method and more stable measurement compared to needle electrode arrays [2]. Thus, ECoGs have been used to identify epileptic foci for clinical purpose, and have been known as a promising tool for controlling a brain machine interface (BMI) / brain computer interface (BCI) for medical and welfare applications [3]. However, the electrodes on the brain surface are directly wired to a recording PC outside of body, and the recording is limited generally within 2 weeks due to its infection risk. So, for further improvement of ECoG-based BMI, it is indispensable to implant all the devices within the patient's head and abdomen. Therefore, we are developing a fully-implantable wireless system to record ECoGs for clinical BMI.

Kojiro Matsushita is with Osaka University Medical School, 2-2 Yamadaoka, Suita-shi, Osaka, 565-0871 JAPAN (corresponding author to provide e-mail: matsushita@nsurg.med.osaka-u.ac.jp).

Masayuki Hirata, Shyne Moriss, Toshiki Yosimine are also with Osaka University Medical School, (e-mail:{masayuki|shayne.morris|yoshimine}@nsurg.med.osaka-u.ac.jp).

Takafumi Suzuki and Hiroshi Ando are with NICT, 2-1 Yamadaoka, Suita-shi, Osaka, 565-0871 JAPAN (e-mail: {t.suzuki|h.ando}@nict.go.jp).

Yuki Ota, Fumihiro Sato, Hideki, Matsuki are with Tohoku University Graduate School of Engineering, (e-mail: {yuki.o|fsato|matsuki}@ecei.tohoku.ac.jp).

Takeshi Yoshida is with Hiroshima Univ., Graduate School of Advanced Sciences of Matter. (e-mail: tyoshida@dsl.hiroshima-u.ac.jp).

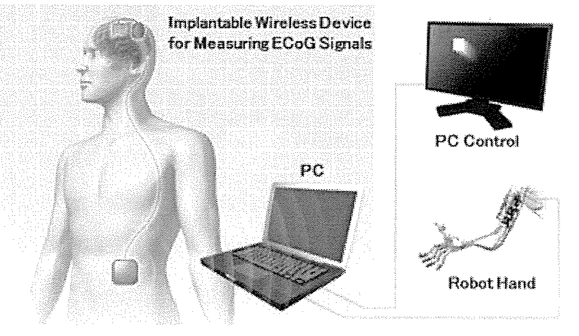

Figure 1. Conceptual Diagram of Clincal BMI

II. 2ND PROTO-TYPE

This is our second proto-type. The device is placed into head, abdomen, and out of body, as shown in Fig.2 and Table 1. The reason that the wireless controller is located in abdominal part is to prevent the user's brain from wireless effects. The head part and the abdominal part are connected with 10 fine cables under the skin. The data communication and power supply are wirelessly conducted so that the in-body devices are fully implanted. The 2nd proto-type is shown in Fig.3 and Fig.4.

The device consists of 5 components: the head part contains 3D highly dense multiple-electrodes, ECoG measuring circuits, and a titanium skull case; the abdominal part contains a Wifi controller and the receiver of a wireless power supply; the out-of-body parts contains the transmitter of a wireless power supply. Table 2 lists those developers.

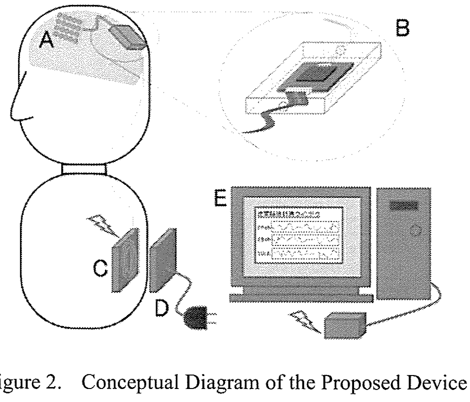

Figure 2. Conceptual Diagram of the Proposed Device

978-1-4577-0216-7/13/$26.00 ©2013 IEEE

TABLE I. LOCATIONS OF DEVEICE PARTS

	Name	Location
A	High-Density Multiple-Electrode Sheet	Head
B	ECoG Measuring Circuit in a Titanium Case	
C	Wireless Controller with Wireless Power Supply (Receiver)	Abdomen
D	Wireless Power Supply (Transmitter)	Out of the Body
E	PC with a Wifi Access Point	

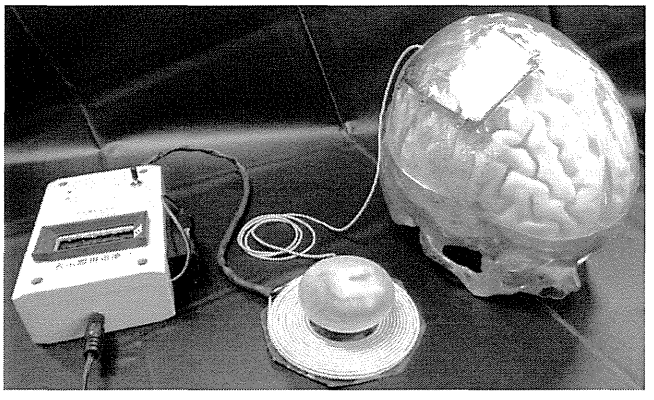

Figure 3. Appearance of the 2nd Proto-type

TABLE II. LIST OF DEVELOPERS

Parts	Developers
3D Highly Dense Multiple Electrodes	Unique Medical Corporation & Shyne Moriss (Osaka Univ.)
ECoG Measuring Circuit	A-R-Tec Corporation & Takeshi Yoshida (Hiroshima Univ.) & Hiroshi Ando (NICT)
Titanium Skull Case	Asuka Denki Seisakujo Corporation & Masayuki Hirata (Osaka Univ.)
Wifi Controller	Hitachi Corporation
Wireless Power Supply	Yuki Ota, Fumihiro Sato, Hidetoshi Matsuki (Tohoku University)
Assembling & Performance Investigation	Takafumi Suzuki (NICT) & Kojiro Matsushita (Osaka Univ.)

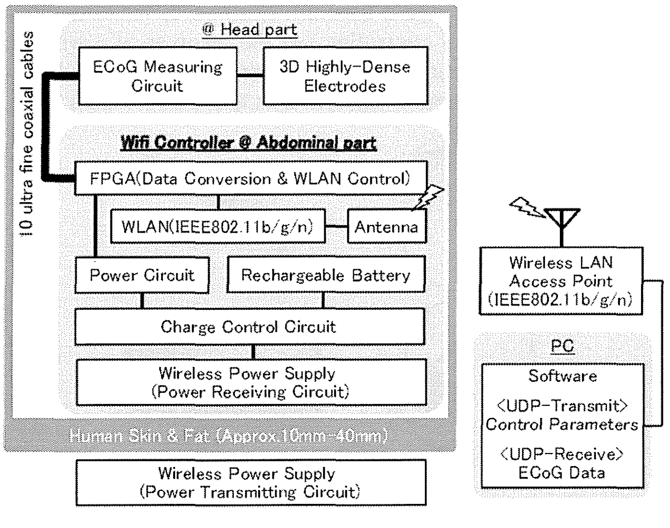

Figure 4. System Architecture of the 2nd Proto-type

III. DETAIL OF DEVICE PARTS

A. 3D Highly-Dense Multiple Electrodes

The proposed electrodes are designed for higher spatial resolution and better signal-to-noise ratio compared to the conventional electrodes (i.e., the conventional electrode is 3.0 [mm] in diameter, and the array is made of the electrodes at 10 [mm] intervals as shown in Fig.5 (left). Therefore, we made a grid electrode of 1.0 [mm] in diameter, and the array contains approx. 100 electrodes at 2.5[mm] intervals. We confirmed that it fits to human brain surface as shown in Fig.5 (right).

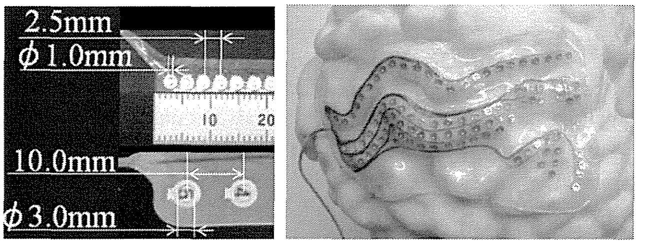

Figure 5. Appearance of the 3D Highly Dense Multiple Electrodes

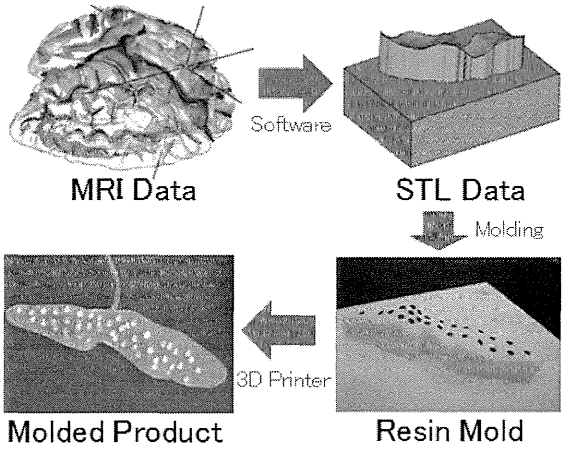

Figure 6. Fabric Process of the 3D Highly Dense Multiple Electrodes

B. ECoG Measuring Circuit

The ECoG measuring circuits are shown in Fig.7. One circuit functions 64 [ch] analog amplifiers and 12 [bit] A/D converters at the maximum sampling rate of 1 [kHz]. Then, we use two circuits at once, in order to deal with 128 [ch] ECoG signals. The specification of the ECoG measuring circuit is listed in Fig.8 and Table 3.

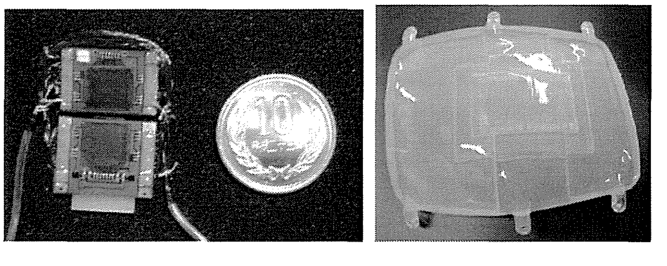

Figure 7. Appearance of the ECoG Meauring Circuits. The right figure shows the location of the circuits inside of the skull case.

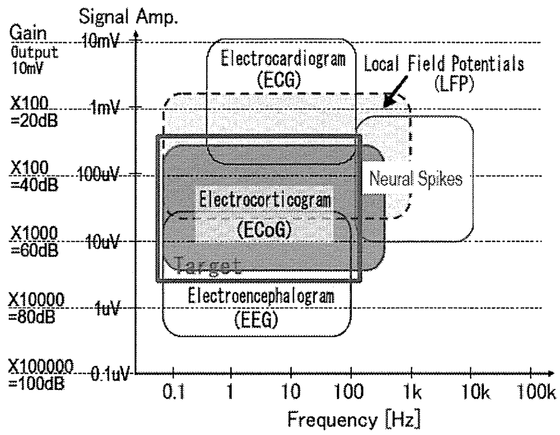

Figure 8. Target Range of the ECoG Measuring Circuit

TABLE III. SPECIFICATION OF ECOG RECORDING CIRCUITS

Name	Specifications
Number of Input Channel	128[ch] (64 [ch] / 1 chip)
Low Pass Filter	0.1 / 1 / 10 [Hz]
High Pass Filter	240 / 500 / 1000 [Hz]
Amplifier Gain	40 / 50 / 60 / 70 / 80 [dB]
Input Voltage Range	1[uV] to 1 [mV]
Sampling Rate	200 / 500 / 1000 [Hz]
Power Consumption	10 [uW/ch]
Circuit Size	28.5mm*19.4mm*5mm

C. *Titanium Skull Case*

We developed a titanium skull case, which contained a 128ch-ECoG measuring circuits. This case functioned as both protecting the circuits and substituting an artificial skull bone. The case is fabricated as follows: (1) We acquire the target patient's head MRI data; (2) We convert MRI data (DICOM data) to 3D model data, extract one part of the skull, design a circuit location; (3) Finally, the skull case is cut out from a titanium block with the CAD data.

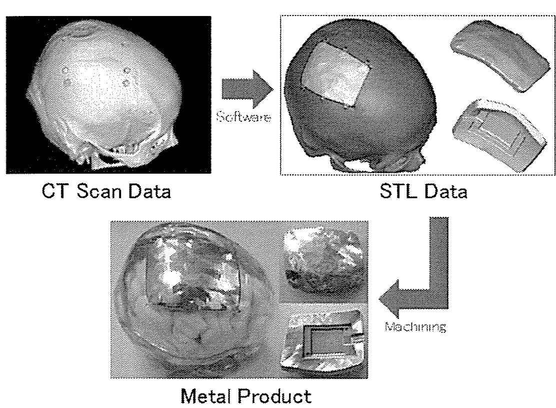

Figure 9. Fabric Process of the Titanium Skull Case

D. *Wireless Controller*

We adapted the Wifi for the second prototype. Our Wifi chip achieves 16Mbps as the maximum data transmission rate, which allowed the transfer of 128-ch * 12-bit ECoG data * 1kHz in real time. Max power consumption was approximately 200 mW, which meant that most of the system power was consumed by the wireless data transfer. The size was 40 mm * 40 mm * 5 mm, as shown in Fig.10.

The abdominal device is based on the wireless controller as shown in Fig.11.

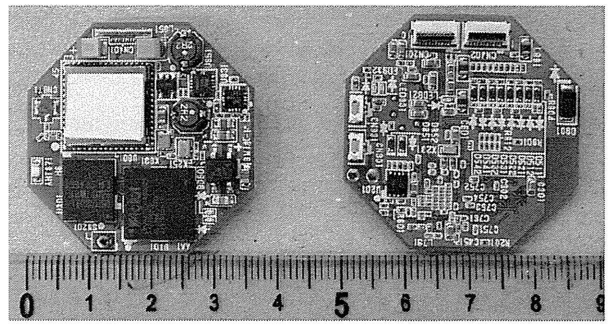

Figure 10. Appearance of the Wireless Controller

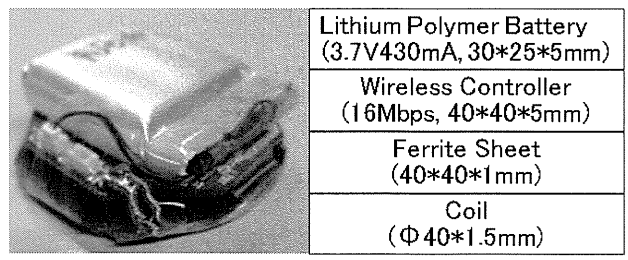

Figure 11. Abdomenal Device, which consists of a wireless controller, a lithium polymer battery, a fferrite sheet, a coil.

E. *Wireless Power Supply*

The wireless power supply consists of two parts. One is a transmitter positioned outside of the human body (Fig.12 left), and the other is a receiver located inside the human body (Fig.12 right). The specification is listed in Table 4. We achieved a wireless power supply of 400 [mW] at a distance of 20 [mm], which was sufficient to run the entire implantable device.

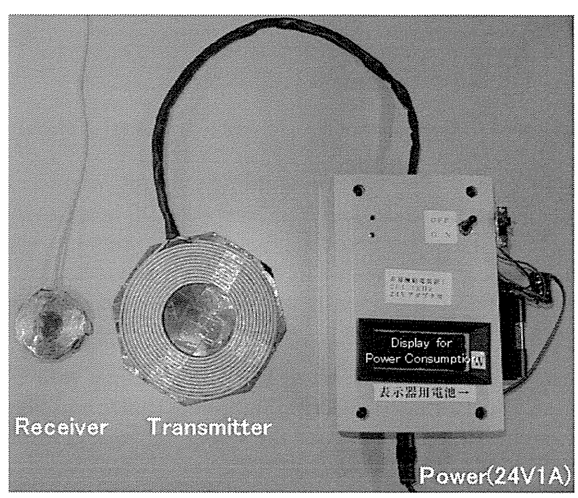

Figure 12. Table 4 Specification of a Wireless Power Supply.

TABLE IV. SPECIFICATION OF THE WIRELESS POWER SUPPLY

Target Distance between coils	20mm
Transmitter Power	400mW
Receiver Coil Size	40mm*40mm*2mm
Transmitter Coil Size	100mm*100mm*5mm
Max. Temperature of Receiver	38 degree

E. Recharging Battery

At the second proto-type, we use the lithium polymer battery (3.7V430mA).We have proved that the battery lasts approx.6 hours to record ECoG signals. We also exchange to bigger battery if ignoring the size.
However, the lithium polymer battery is not proved as its bio-compatibility so that we need to look for implantable batteries and substitute for it.

TABLE V. SPECIFICATION OF THE RECHARGING BATTERY

Battery capacity	3.7V430mA
Estimated power consumption of the whole system	Average 80mW (Max. 200mW)
Estimated working time	Approx. 6 hours

IV. PERFORMANCE TEST

We are now conducting animal experiments with the device shown in Fig.13. It is designed for monkeys so that it functions only 64ch: in short, it consists of a 64ch flat highly-dence multiple electrodes, a titanium skull case, and one ECoG measuring circuit.

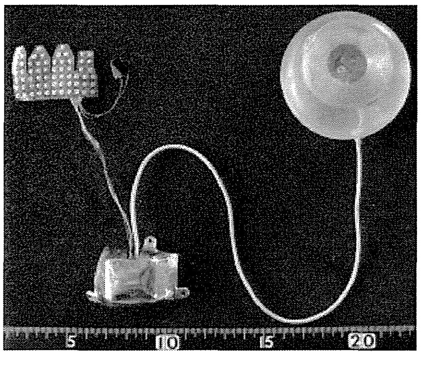

Figure 13. Appearance of the Implantable Device for a Monkey

Fig.14 shows the battery condition when we wirelessly supply power to the device. It takes approx.10 hours to the full condition. This is because that we temporally set the recharging current low due to keeping the device safe. Then, after recharging, it demonstrated that the device lasts approx. 6 hours.

Fig 15 illustrates one result of ECoG recordings with GAIN: 80db, Cut-off Freq.: 1-240Hz, Sampling:1kHz, and Num. of Ch.: 64ch , Distance between the implantable device and the recording PC: 3m.

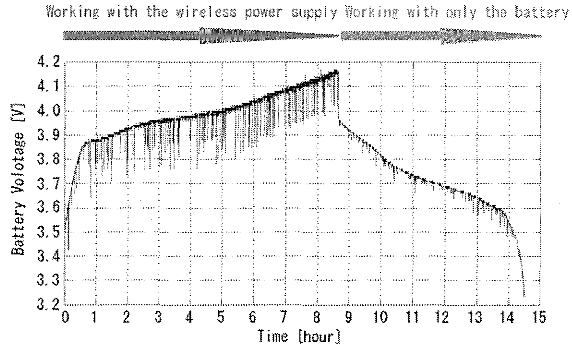

Figure 14. Investigation on the battery condition

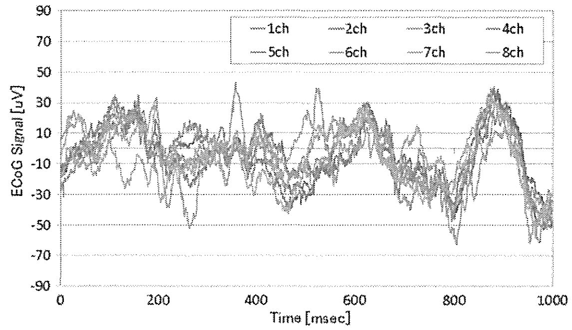

Figure 15. Example of ECoG recording data (displaying only 8ch)

V. CONCLUSION

Due to reducing the infection risk and achieving long-term ECoG measurement, we are developing a fully-implantable wireless ECoG recording device. In this paper, we introduced our 2nd proto-type: the 3D highly-dense multiple electrodes, the ECoG measuring circuits, the titanium skull case, the wireless controller, the wireless power supply. We have investigated those performances, and are trying animal experiments.

ACKNOWLEDGMENT

This work was supported in part by the Strategic Research Program for Brain Sciences, and the Translational Research Network Program by the Ministry of Education, Culture, Sports, Science and Technology (MEXT) Japan, by KAKENHI (22390275, 23390347) by Japan Society for the Promotion of Science (JSPS), and by Health Labour Sciences Research Grant (23100101) by the Ministry of Health Labour and Welfare.

REFERENCES

[1] Schlogl et al., 2005 A. Schlogl, F. Lee, H. Bischof and G. Pfurtscheller, Characterization of four-class motor imagery EEG data for the BCI-competition 2005, J. Neural. Eng. 2 (2005), pp. L14–22.
[2] Meel Velliste, Sagi Perel, M. Chance Spalding, Andrew S. Whitford and Andrew B. Schwartz, Cortical control of a prosthetic arm for self-feeding, Nature,doi:10.1038/nature06996, 2008.
[3] Takufumi Yanagisawa, Masayuki Hirata ,Youichi Saitoh, Amami Kato, Daisuke Shibuya, Yukiyasu Kamitani, and Toshiki Yoshimine. Neural decoding using gyral and intrasulcal electrocorticograms. NeuroImage Volume 45, Issue 4, p.p. 1099-1106.

Behavioural Neurology 27 (2013) 229–234
DOI 10.3233/BEN-110249
IOS Press

Case Report

Possible roles of the dominant uncinate fasciculus in naming objects: A case report of intraoperative electrical stimulation on a patient with a brain tumour

Keiko Nomura[a], Hiroaki Kazui[a,*], Hiromasa Tokunaga[a], Masayuki Hirata[b], Tetsu Goto[b], Yuko Goto[b], Naoya Hashimoto[b], Toshiki Yoshimine[b] and Masatoshi Takeda[a]
[a]*Department of Psychiatry, Osaka University Graduate School of Medicine, Suita-city, Osaka, Japan*
[b]*Department of Neurosurgery, Osaka University Graduate School of Medicine, Suita-city, Osaka, Japan*

Abstract. How the dominant uncinate fasciculus (UF) contributes to naming performance is uncertain. In this case report, a patient with an astrocytoma near the dominant UF was given a picture-naming task during intraoperative electrical stimulation in order to resect as much tumourous tissues as possible without impairing the dominant UF function. Here we report that the stimulations with the picture-naming task also provided some insights into how the dominant UF contributes to naming performance. The stimulation induced naming difficulty, verbal paraphasia, and recurrent and continuous perseveration. Moreover, just after producing the incorrect responses, the patient displayed continuous perseveration even though the stimulation had ended. The left UF connects to the inferior frontal lobe, which is necessary for word production, so that the naming difficulty appears to be the result of disrupted word production caused by electrical stimulation of the dominant UF. The verbal paraphasia appears to be due to the failure to select the correct word from semantic memory and the failure to suppress the incorrect word. The left UF is associated with working memory, which plays an important role in recurrent perseveration. The continuous perseveration appears to be due to disturbances in word production and a failure to inhibit an appropriate response. These findings in this case suggest that the dominant UF has multiple roles in the naming of objects.

Keywords: Left uncinate fasciculus, naming objects, awake surgery, intraoperative electrical stimulation, low-grade astrocytoma

1. Introduction

The uncinate fasciculus (UF) is a white matter tract that connects the inferior frontal lobe with the anterior inferior temporal lobe [1]. A tumour resection study revealed that the left UF is essential for naming common objects [2]. Also, a diffusion tensor imaging (DTI) study found that demyelination and axonal injury of the left UF were associated with a decline in naming performance [3]. Although these two studies suggested that the left UF is associated with naming performance, they have a few shortcomings. In the tumour resection study, not only the left UF but also a part of the surrounding cortical regions was resected [2]. In the previous DTI study, the patients had temporal lobe epilepsy [3], which is likely to cause atypical language lateralization [4]. In addition, the DTI study did not assess whether the left UF was associated with symptoms that are related to naming deficits, such as paraphasia, perseverations, and speech arrest [3].

*Corresponding author: Hiroaki Kazui, M.D., Ph.D., Department of Psychiatry, Osaka University Graduate School of Medicine, D3 2-2 Yamadaoka, Suita-city, Osaka, 565-0871, Japan. Tel.: +81 6 6879 3051; Fax: +81 6 6879 3059; E-mail: kazui@psy.med.osaka-u.ac.jp.

ISSN 0953-4180/13/$27.50